A review of excimer laser projection lithography

M. Rothschild and D. J. Ehrlich

Citation: Journal of Vacuum Science & Technology B: Microelectronics Processing and Phenomena **6**, 1 (1988); doi: 10.1116/1.584004

View online: https://doi.org/10.1116/1.584004

View Table of Contents: https://avs.scitation.org/toc/jvm/6/1

Published by the American Institute of Physics

ARTICLES YOU MAY BE INTERESTED IN

Extreme ultraviolet lithography: A review
Journal of Vacuum Science & Technology B: Microelectronics and Nanometer Structures Processing, Measurement, and Phenomena **25**, 1743 (2007); https://doi.org/10.1116/1.2794048

Extreme ultraviolet lithography and three dimensional integrated circuit—A review
Applied Physics Reviews **1**, 011104 (2014); https://doi.org/10.1063/1.4863412

A review of ion projection lithography
Journal of Vacuum Science & Technology B: Microelectronics and Nanometer Structures Processing, Measurement, and Phenomena **16**, 927 (1998); https://doi.org/10.1116/1.590052

Nanoimprint lithography: An old story in modern times? A review
Journal of Vacuum Science & Technology B: Microelectronics and Nanometer Structures Processing, Measurement, and Phenomena **26**, 458 (2008); https://doi.org/10.1116/1.2890972

A review on the processing accuracy of two-photon polymerization
AIP Advances **5**, 030701 (2015); https://doi.org/10.1063/1.4916886

Nanofabrication by scanning probe microscope lithography: A review
Journal of Vacuum Science & Technology B: Microelectronics and Nanometer Structures Processing, Measurement, and Phenomena **23**, 877 (2005); https://doi.org/10.1116/1.1926293

Critical Review

A review of excimer laser projection lithography

M. Rothschild and D. J. Ehrlich
Lincoln Laboratory, Massachusetts Institute of Technology, Lexington, Massachusetts 02173

(Received 31 July 1987; accepted 20 October 1987)

Excimer-laser projection lithography now appears to be in a position to extend production optical techniques to dimensions approaching 0.25 μm. Such methods could well be the basis for the bulk of the advanced manufacturing capability in microelectronics over the next decade. This technology is reviewed with an eye to the state of the art and to the optical-, resist-, and materials-engineering issues that it presents.

I. INTRODUCTION

In this paper we review the early status of excimer laser projection lithographies. Although these technologies have been under moderately paced development since[1] 1982, only this year have their special power and significance to the future of microfabrication become widely recognized.[2] It now appears that, with some further development, this relatively overlooked new technology may provide the bulk of the production capacity for the microelectronics industry over the next decade. Specifically, it is fully foreseeable that it is with this technology that optical techniques can be extended to achieve production throughputs at dimensions approaching 0.25 μm, well into the regime reserved as recently as last year for x-ray and particle-beam lithographies. It is also possible that it is this technology that will be the ultimate optical technique, reaching the point where fundamental materials limitations will finally mandate a departure from optical lithographies.

The demands on future lithographies are intense. At the time of this writing, 4-Mbit dynamic random access memories (DRAMs) can be produced using commercial step-and-repeat systems, without subfield stitching. This task already requires the most nearly perfect wide-field imaging optics in existence for any commercial purpose. 16-Mbit and 32-Mbit chips will require $\sim 10^9$ pixels in an optical field, two to four times that of these systems. As will be shown below, the challenge of developing the appropriate ultraviolet (UV) excimer projection system is far from trivial.

On the basis of general considerations, higher resolution optical projection lithographies can be achieved by a combination of the following approaches: increasing the numerical aperture (NA), shortening the wavelength, and inventing resists with highly nonlinear photoresponses. In choosing between these directions it is noted that the major practical source of error for an aberration-free optical projection system is defocusing, the latitude for which scales inversely with the square of the numerical aperture. After a point, wafer topography mandates reducing the wavelength rather than increasing the numerical aperture, as will be discussed later. In keeping with this, projection printers have been progressively designed without significant increase in NA to operate at 436 nm, then at 405 nm, and more recently at 365 nm. These are the G, H, and I lines, respectively, in the high-pressure mercury lamps commonly used as the photon source in projection printers. Significant work has also been done in improving photoresists. A major constraint, however, has been the need to obtain high-sensitivity materials to be used with relatively weak irradiation from lamps. In practice, sensitivity is difficult to obtain and optimization of the nonlinearity of the response has been relatively imperfect. Incremental improvements to current lamp-based lithographies may bring the latter asymptotically to the vicinity of $\sim$0.5-μm linewidths; however, further progress requires a more revolutionary modification of projection printers. This change is now widely speculated to be the replacement of the mercury lamp with an excimer laser as the photon source.

Such a change will have several benefits. The immediate, and more obvious one, is improved resolution due to the shorter wavelength. Excimer lasers operate at several wavelengths, the most common ones being 351 (lasing species XeF), 308 (XeCl), 248 (KrF), and 193 nm (ArF). As outlined below, even the shortest of these wavelengths allows for a defocusing tolerance > 1 μm at NA $= 0.3$, while at the same time the diffraction-limited cutoff linewidth is reduced to less than one-half that of the mercury G and H lines.

Moreover, the short wavelength of excimers may open opportunities for direct (resistless) dry patterning technology. This comes about because, at these new higher photon energies, numerous compounds undergo efficient photochemistry. It is highly likely that the excimer laser will go beyond the traditional role of the lamp and may *itself* serve as an energy source to drive chemical processing, e.g., deposition, etching, and doping.

A final property with important implications is the high peak intensity of excimer lasers. Mercury lamps are continuous sources delivering fluxes in the 1 W cm^{-2} range. Excimer lasers, on the other hand, operate in the pulsed mode (10–25 ns pulse width), delivering fluxes over cm^2 areas which are easily 10^7 times higher. This dramatic difference in flux, coupled with the shorter wavelength of the excimer laser, has important implications for integrated circuit processing with resists. Nonlinear processes can now be induced in numerous materials with great efficiency. Therefore, the concern with resist photosensitivity, which is dominant in lamp systems, may become of secondary importance. Instead, new resists can be employed with properties such as dry processibility, self-development, bleaching, and high contrast. In particular, acceptable levels of the intensity

 0734-211X/88/010001-17$01.00 © 1988 American Vacuum Society

modulation in the image plane can be reduced well-below the common requirements (usually ~0.7). It thus becomes possible to operate the projection system closer to the high-spatial-frequency cutoff, further enhancing the resolution to linewidths possibly below 0.2 μm. This last dimension has in fact already been achieved in the laboratory.[3]

The great potential of excimer lasers in photolithography is at present tempered by a number of not yet fully solved challenges. Foremost of these is the availability of aberration-free projection optics in the UV. The design of such optics must take into account the specific adjustable output properties of the laser, such as spectral linewidth and spatial coherence and uniformity. The high peak intensity may cause catastrophic damage to optical elements; the high average power may generate absorption in nominally transparent materials. Direct processes necessitate low values of peak power in order to avoid surface damage. This may reduce the throughput to unacceptably low levels, unless changes are introduced in present excimer laser technology. Laser sources must operate with the high degree of reliability required in integrated circuit production lines. Unfortunately, these technological issues grow in complexity as the wavelength is shortened.

In the following sections we will review recent developments in the field of excimer projection. In Sec. II we will discuss the optical aspects that need to be considered in an excimer stepper. In Sec. III we will outline some general considerations, as well as detail specific examples of laser/material responses as they apply to excimer projection patterning. We draw upon our own results and those of other researchers. In the final section we summarize the current status and direction of the technology.

II. OPTICAL CONSIDERATIONS

A. General

We begin with a discussion of the design considerations for the optical systems to be used with excimer sources. Key issues are resolution, depth of focus, and the trade-off in optimization of these two quantities, control of chromatic aberration, and the new considerations in coherence of illumination introduced by excimer sources. We treat these questions below.

B. Resolution and depth of focus

The smallest dimension that can be generated by an optical imaging system is ultimately limited by diffraction. In the case of imaging of equal lines and spaces with incoherent light, for instance, the absolute cutoff linewidth is $d_{co} = \lambda/4$ NA, where λ is the wavelength and NA is the numerical aperture in the image space. Of course, several factors, particularly resist response, limit useful resolution to well short of this value; the smallest linewidth is typically $> 3 d_{co}$. Nevertheless, d_{co} is a useful quantity in evaluating the optical limitations of a projection printer. From the expression for d_{co} it follows that higher resolution may be achieved by reducing λ or increasing NA. However, changing either one of these parameters automatically affects another quantity, namely, the depth of focus. A measure of the acceptable tolerance on defocusing is the Rayleigh range, $z_d = \lambda/2(\mathrm{NA})^2$. Although optical projection systems are frequently designed to operate at near theoretical diffraction-limited performance, in practice, defocusing is a major source of degradation. Defocusing is the result of several factors[4]: focusing error, wafer nonflatness over the field of view, and imperfect planarization between lithographic steps. A common minimum focal latitude in current manufacturing practice is 0.8–1.0 μm. Figure 1 represents the interplay between d_{co} and z_d for different wavelengths and numerical apertures. In Fig. 1, a set of values of λ and NA determines a point, whose coordinates are d_{co} and z_d. The solid line segments represent existing steppers[5] operating at 436 and 365 nm with NA in the range of 0.30–0.45. On the basis of the relationships of Fig. 1, the preferred trend is to achieve smaller d_{co} by reducing the wavelength rather than increasing the numerical aperture in order to lessen the decrease in z_d. For instance, in order to achieve $d_{co} = 0.2$ μm (corresponding to a practical minimum feature size of $\sim 3\ d_{co} = 0.6$ μm), a *G* line stepper at 436 nm has to be operated at the relatively high NA = 0.55, with a $z_d = 0.73$ μm, while a KrF laser stepper at 248 nm can have more relaxed values of NA = 0.31 and $z_d = 1.3$ μm.

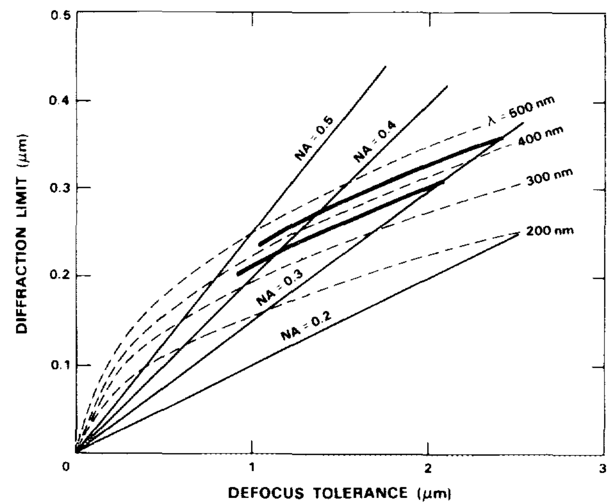

FIG. 1. The diffraction limited linewidth d_{co} and the defocusing tolerance z_d as functions of the wavelength λ and numerical aperture NA. For any imaging system, d_{co} and z_d are the coordinates of the point determined by the intersection of the appropriate λ curve and NA curve. The solid line segments represent the operating parameters of existing Hg-lamp steppers at $\lambda = 436$ and $\lambda = 365$ nm, with NA in the range 0.30–0.45.

The information presented in Fig. 1 can also be cast in a different way. If one assumes that because of practical constraints in any stepper, $z_d \geqslant 0.8$ μm and NA $\leqslant 0.45$, then d_{co} assumes the values 0.21, 0.19, 0.16, and 0.14 μm for *G* line, *I* line, KrF laser, and ArF laser steppers, respectively. The lithographic dimension (using the factor of 3 mentioned above) can be lowered from 0.62 μm at 436 nm, to 0.48 and 0.42 μm, respectively, at the two excimer wavelengths. Even without postulating improved resists, this reduction is equivalent to a shrinkage of 23% and 33%, respectively, in the linear dimension of the printable element size.

These figures provide a strong motivation for replacing mercury lamps with short-wavelength excimers. However, as the following sections will show, the degree of difficulty in carrying out this transition also increases as the wavelength becomes shorter.

C. Chromatic aberration

Excimer lasers operate on bound-to-dissociative molecular transitions, which have significant spectral width. Free-running ArF lasers have a spectral width of ~ 100 cm^{-1}, and the KrF laser output is ~ 50 cm^{-1} wide.[6] The XeCl and XeF lasers, because of the weakly bound nature of their ground states, exhibit (in their free-running mode) several sharper vibrational lines superimposed on a weak continuum.[7] This spectral width causes a significant chromatic spread in the best focus of the projection system. The effect of large bandwidth of excimer lasers is further compounded by the fact that the dispersion of most optical materials increases rapidly with decreasing wavelength. For fused silica, for instance, the refractive index at 193 nm varies across the 100 cm^{-1} width of ArF lasers by $\delta n_{\text{ArF}} \approx 6.2 \times 10^{-4}$, while at 248 nm it varies across the 50 cm^{-1} of the KrF laser by $\delta n_{\text{KrF}} \approx 1.7 \times 10^{-4}$. If a fused silica lens is used for projection, these values of δn cause a spread in focal length δf given by

$$\delta f = f \delta n/(n-1), \quad (1)$$

where f is the focal length and n is the (mean) refractive index. Even with a conservatively short focal length $f = 1$ cm, the spread assumes the values $\delta f_{\text{ArF}} \approx 11$ and $\delta f_{\text{KrF}} \approx 3.4$ μm, which are much larger than the defocusing tolerance discussed in Sec. II B. While the above treatment deals only with primary chromatic aberration, the laser bandwidth further degrades the image quality via higher order aberrations such as spherochromaticity. It is therefore obvious that, because of the combined effect of large free-running bandwidth and high dispersion, chromatic aberrations must be addressed in projection systems using excimer lasers.

With refractive optics, δf can in principle be reduced by either spectral narrowing of the excimer laser output, or by achromatization of the projection lens. Both approaches have recently been applied to the development of steppers at 248 nm. The first method, applied by Pol *et al.*[8] and Endo *et al.*,[9] introduces a degree of complexity in the laser end of the projection system. For instance, the bandwidth of KrF lasers can be reduced to < 1 cm^{-1} with the use of intracavity étalons or with injection locking in an oscillator–amplifier configuration. In either case there are certain drawbacks, such as reduced energy output or lower pulse repetition rate. The second approach, applied by Nakase *et al.*[10] and by Kameyama and Ushida,[11] employs free-running lasers at the price of a more complex and more damage-prone projection lens. The design and production of achromats in the visible is by now a routine task because of the availability of glasses with varying refractive indexes and dispersive properties. In fact, achromats are employed in Hg-lamp projection systems, where pressure broadening results in several-nm-wide output lines. At the excimer laser wavelengths, however, there is a limited selection of transparent materials. These include fused silica and several metal fluorides, mainly calcium, magnesium, and lithium. A projection lens which is achromatic over the laser bandwidth can indeed be designed using two or more of these materials. Unfortunately, they all have certain undesirable properties. For instance, LiF is hygroscopic, and MgF_2 is birefringent. All, and in particular CaF_2, develop color centers due to minute amounts of impurities, when exposed to high doses of laser radiation. It should also be noted that both the difficulties encountered in line narrowing the laser and the propensity of materials toward developing color centers quickly increase at the shorter wavelengths.

Irrespective of the scheme to overcome chromatic aberrations, refractive optics are also sensitive to ambient temperature fluctuations. The temperature should be stabilized within tolerances determined by allowable temperature-induced variations in focal length $\delta f < 0.1\, z_d$. For fused silica, the temperature coefficient of the index of refraction is $dn/dT \approx 1.8 \times 10^{-5}$ K^{-1} at 248 nm and $dn/dT \approx 2.2 \times 10^{-5}$ K^{-1} at 193 nm. For $z_d = 1$ μm, $\delta f < 0.1$ μm implies the rather stringent requirement of $\delta T < 0.25$ K for practical focal lengths at these two wavelengths.

A different way to eliminate chromatic aberrations is the use of a projection lens made of reflective elements, since mirrors are systems intrinsically free of chromatic aberrations at all wavelengths. Reflective optics have been employed in scanning projection systems with 1:1 imaging using a XeCl laser.[12] For finer patterning, however, steppers with some demagnification seem to be more appropriate. An example of such a lens is the Schwarzschild microscope objective which we have used extensively in our own narrow-field-of-view studies of projection lithography.[3,13] These optics, based on a simple two-mirror imaging system, is shown in Fig. 2. At present, reflective optics, as well as catadioptric systems, are not yet fully developed candidates for projection objectives in commercial excimer-based steppers.

D. Spatial coherence

Conventional projection printers are designed to operate with partially coherent illumination, i.e., with a certain amount of statistical correlation between the optical field at various points in the object (mask) and image (wafer)

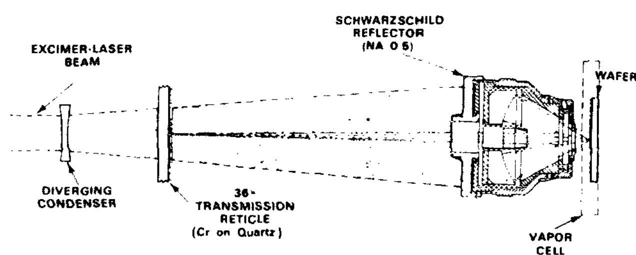

FIG. 2. Original Schwarzschild-objective imaging system for the first submicrometer-resolution excimer projection experiments (see Ref. 13). The reflective design allowed imaging wavelengths shorter than those permitted by the large-NA refractive optics of the time. Experiments were carried out to wavelengths as short as 157 nm. The record for high resolution at the time of writing (0.13-μm lines and spaces) is still held by a version of this system.

planes. Although from a practical standpoint the raw lamp output is totally incoherent, some coherence at the mask is imposed by the finite size of the condenser and objective. The parameter σ, defined in terms of the cutoff in the spatial spectral density of the optical field and approximately equal to the inverse of the correlation length of the optical field normalized to λ /NA, is often taken as a measure of the departure from coherence. The value of σ is determined by the numerical apertures of the two lenses:

$$\sigma = NA_{condenser}/NA_{objective}, \quad (2)$$

where both NA's are in the object (mask) space. The two extreme values of σ are $\sigma = 0$, corresponding to the coherent limit when the lamp is effectively a point source, and $\sigma \to \infty$, corresponding to the incoherent limit when the lamp is an infinitely large plane source. In projection printers, σ has intermediate values, typically in the range 0.4–0.8. The degree of coherence to be employed has major implications in the design of excimer projection optics and we, therefore, consider this issue in some depth below.

A common mode of analysis in incoherent imaging involves the effect of the optical system on the various Fourier terms of the object, described in terms of a modulation transfer function (MTF), which is the ratio of the contrast in the image plane to that in the object. For a high-contrast one-dimensional object the MTF may be defined as:

$$MTF(\xi) = \frac{I_{max}(x) - I_{min}(x)}{I_{max}(x) + I_{min}(x)} \leqslant 1, \quad (3)$$

where ξ is the frequency and $I(x)$ is the intensity distribution in the image plane.

The fact that the MTF is a meaningful and useful quantity in incoherent imaging follows from the fact that (a) the physically significant quantity in incoherent light is its intensity, and (b) both the Fourier transform and the effects of the optical system are linear in intensity. With partially coherent illumination, however, both the amplitude and the phase of the illuminating wave front participate in the image-forming process. The MTF is no longer a universal, single-valued function of frequency.[14] Nevertheless it has remained the most customary characterization of stepper objective optics[15] and we retain it for our discussion. Figure 3 shows the results of calculations assuming a one-dimensional lens, and a one-dimensional object[16] whose *amplitude* distribution is

$$A(x') = \tfrac{1}{2}[1 + \cos(2\pi\xi' x')]. \quad (4)$$

This describes a high-contrast single-frequency object with no phase modulation, as is typical in lithography. The intensity in the image plane is given by

$$I(x) = F_1 + F_2 \cos(2\pi\xi x) + F_3 \cos(4\pi\xi x). \quad (5)$$

The quantities F_1, F_2, F_3 are functions of the normalized spatial frequency ξ as well as of the degree of coherence σ. $I(x)$ contains more than one spatial frequency. The MTF [Eq. (3)] becomes

$$MTF = F_2(\xi)/[F_1 + F_3(\xi)], \quad (6)$$

where the value of MTF pertains only to the particular object Eq. (4). In Fig. 3, this MTF was calculated for three values of σ: 0.2, 0.5, and 2.0, corresponding to highly coherent, intermediate, and highly incoherent illumination. The effects of defocusing error on an aberration-free system were examined by calculation of three cases: $z_d = 0, \lambda/2(NA)^2$, and $\lambda/(NA)^2$. While certain details of the results may vary from object to object, the qualitative features in Fig. 3 are quite general. In perfect focusing ($z_d = 0$), the more coherent illumination yields a higher MTF for $\xi < NA/\lambda$, and lower MTF for $\xi > NA/\lambda$. Also, coherent illumination is less sensitive to defocusing. For instance, at $\xi = NA/\lambda$, a defocusing error of $\lambda/2(NA)^2$ results in the MTF being reduced from 0.65 to 0.32 at $\sigma = 2$, but only slightly changed (from 0.65 to 0.62) at $\sigma = 0.2$. In general, the larger z_d, the smaller the range of frequencies over which incoherent imaging has a higher MTF than coherent imaging. It should be noted that ξ and z_d are normalized in terms of λ and NA, and therefore the same expression may have different numerical values in different systems. For instance, the frequency $\xi = NA/\lambda$ is 0.80 μm^{-1} for a G line projection system ($\lambda = 0.436\ \mu m$) with NA = 0.35, and 1.6 μm^{-1} for an ArF-excimer projection lens ($\lambda = 0.193\ \mu m$) with NA = 0.30. Similarly, the defocusing $z_d = \lambda/2(NA)^2$ has the numerical values 1.78 and 1.07 μm in the two systems, respectively.

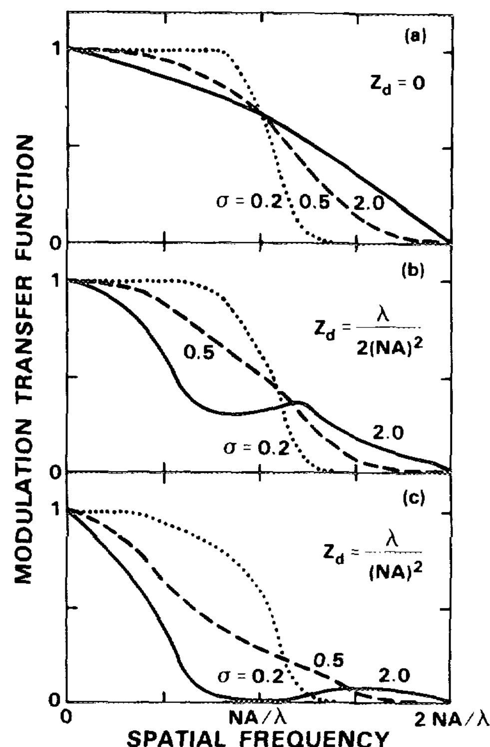

FIG. 3. The effects of spatial coherence and defocusing on resolution, as determined by the modulation transfer function (MTF) for the periodic object represented by Eq. (4). The MTF curves were calculated for three values of the degree of spatial coherence, σ: $\sigma = 0.2$ (highly coherent) $\sigma = 0.5$ (intermediate), and $\sigma = 2.0$ (highly incoherent). In (a) perfect imaging is assumed (defocusing tolerance z_d is zero), and in (b) and (c) defocusing of one and two Rayleigh ranges, respectively, is introduced in the analysis.

The foregoing analysis may be applied to an isolated edge[17,18] rather than to a periodic object. In this case, the

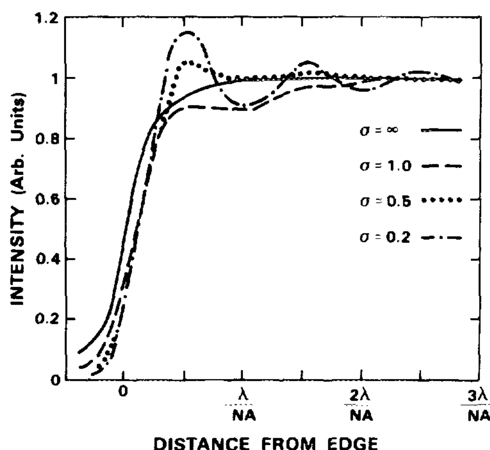

FIG. 4. The intensity distribution in the image plane of a sharp edge, for several values of the coherence parameter σ. For coherent illumination, note the $\pm$ 15% ringing in the illuminated area as well as the lateral shift of $\sim\lambda/4$ NA in the position of the edge (defined as the point of intensity 0.5). On the other hand, incoherent illumination has a significant "toe," i.e., intensity extending $\sim\lambda/4$ NA into the geometrical shadow.

image is sharper with coherent imaging, but it also exhibits intensity "ringing" in the illuminated region as well as a lateral shift of the image from its geometrical position. This case is shown in Fig. 4.

The incorporation of excimer lasers in projection printers adds a new consideration to the control of the degree of spatial coherence. Unlike lamps, excimer lasers possess a certain degree of intrinsic spatial coherence, which is determined by the number and distribution of oscillating cavity modes. Since the number of modes in excimer lasers is very high, the degree of coherence is low. Nevertheless, it may have a profound impact on image quality, as shown below. If no condenser is placed between the laser and the mask, the value of σ is given by[19]

$$\sigma \approx 3m\theta_{\rm div}/{\rm NA}, \quad (7)$$

where $\theta_{\rm div}$ is the divergence half-angle of the laser and m is the magnification. For free-running excimer lasers, $\theta_{\rm div} \approx 4$ mrad. Therefore, for a $10\times$ lens with low numerical aperture of NA = 0.2, we find $\sigma \approx 0.6$, a value which is within the range of σ's of conventional printers. Similarly, for a high-magnification lens such as a $36\times$, 0.5 NA Schwarzschild objective, $\sigma \approx 0.9$, and the illumination approaches the incoherent limit. However, common projection lenses for production steppers typically have high NA and lower magnification, and the resultant value of σ is too low ($\sigma \approx 0.20$ for a $5\times$, 0.3 NA lens), i.e., the illumination is too coherent. Furthermore, if line narrowing is used, as discussed above, the number of spatial modes is typically reduced as well. This manifests itself in a reduced divergence and increased degree of coherence, far beyond its optimal value. In most instances it is therefore necessary to reduce the spatial coherence of the excimer laser before propagating the beam through the rest of the optical system.

Several methods to accomplish this have been reported. At the longer wavelengths (308 nm), Kerth *et al.*[12] placed a quartz diffuser in the beam. A similar effect may be achieved with a randomly oriented fiber bundle. Because of the time-varying nature of the pulsed intensity, these methods are equivalent to a moving diffuser in a cw beam.[20] These are, however, lossy processes, and their application to shorter wavelengths (248, 193 nm) may be impractical because of the low energy throughput of diffusers and fibers. Horiike *et al.*[21] have used a 248 nm diffuser comprising a set of closely spaced ("fly's eye") lenslets. Pol *et al.*[8] employed a different approach, applicable to multiple-pulse exposures, in focusing onto a spot in the object plane of the condenser, i.e., the source plane, and moving this spot in its plane from pulse to pulse.[22] Individual pulses are still coherent. However, the cumulative effect of multiple-pulse exposure is the random superposition of individual speckle patterns, which average out to uniform illumination. This last technique has intriguing possibilities, since it lends itself to dynamic control of σ, via the amount of scanning that is performed in the source plane.

Finally, a major drawback of fully coherent imaging is its high sensitivity to local phase shifts, back reflections, and scattering, which are caused by material imperfections and other spatial inhomogeneities. These shifts lead to undesired coherent noise patterns in the image plane, including speckle. We note that as well as transverse spatial coherence, these noise effects require longitudinal coherence length (temporal coherence) exceeding the path length differences that produce the noise in the image plane. These deleterious effects can become important even at relatively high σ for narrowed bandwidth excimer lasers. At the time of this writing there is not a sufficient understanding of the excimer-laser mode properties to fully predict the requirements on the optics, and their variation with linewidth and number of pulses averaged.

III. MATERIAL RESPONSES

A. General considerations

In the sections above, we have described the factors governing the formation of an optimal aerial image at the wafer plane. In traditional lithographic applications three tasks follow: first, the capture of the aerial pattern as a latent image in photoresist (exposure); second, the transfer of the latent image into resist topography (development); and third, the further transfer of the resist topography onto the wafer by etching or lift-off. This sequence, although rigidly adhered to with lamp-based lithography, is not necessarily followed in excimer projection techniques. The first two of the three operations are sometimes combined to get a "self-developing" response, and all three operations combined for "direct" (resistless) processing. These new capabilities, which simplify microfabrication by eliminating steps, become possible because of the efficiency of pulsed, deep-UV excimer radiation in exciting a vastly broader range of material responses than is feasible with lamps. Indeed, the consideration usually dominant as a first (i.e., most demanding) design criterion for lamp resists, namely sensitivity, is well down on the list for excimer lithography (more on this below). A second prominent criterion, namely profile control

(e.g., via controlled bleaching), often becomes far less important because excimer imaging layers are often thinner than less rugged lamp resists. Below we consider the properties of material responses generated in excimer projection. Since the range of useful responses is much broader than traditionally permitted, and many of the usual constraints are absent, the desired features for imaging materials will be considered from a fairly general point of view.

As is attested to by their success in current practice, traditional resist materials can have excellent performance and are likely to be used widely with excimers. However, even these will be modified before they can be applied to excimer processing. For example, it is widely realized that the most favored current photoresists (Novolak-based systems) are too strongly absorbing in the deep UV. Other properties will also be changed because of the new flexibility. We begin this discussion with definition of parameters and a discussion of general considerations for material systems.

The imaging response of photoresists, exposure and development processes considered together, is generally characterized by a contrast parameter, defined as $\gamma = [\log_{10} \times (E_0/E_1)]^{-1}$ in terms of the quantities specified in Fig. 5. In Fig. 5, the fractional remaining thickness of a positive resist, following exposure and standard development, is plotted as a function of the exposure dose E. The minimal dose for which the remaining thickness is zero is the threshold dose $E = E_0$. The slope at E_0 of the semilogarithmic curve in Fig. 5 determines the dose E_1 at which the tangent attains the ordinate value of 1. Usually, γ has a fairly constant well-defined value over the energy range of use. The value of γ determines the minimum aerial image modulation required of the optics. Typical achieved values are[23] $\gamma = 2.0$–4.5, although it has long been known that greater values would be desirable. Recently, "contrast enhancement" (bleachable) overlayers have been incorporated in some lamp processes.[24] To first order, these are passive in image recording and do not change resist nonlinearity but increase effective γ by biasing the photoresponse curve, Fig. 5, to higher doses for $E < E_0$, while keeping the point $E = E_0$ unchanged. Enhancement factors of ~ 3 are achievable with commercially available contrast enhancement layers.[25]

As a generalization of γ we specify the general response of an excimer material system as follows: The laser-induced process has a rate per pulse $R(\Phi)$ which is a function of the laser fluence Φ. At the operating fluence Φ_0, we set $R(\Phi_0) = R_0$, and for small deviations of Φ from Φ_0,

$$\frac{R(\Phi)}{R_0} \approx 1 + \frac{d(R/R_0)}{d(\ln \Phi)}\bigg|_{\Phi=\Phi_0} \ln(\Phi/\Phi_0) + \cdots$$
$$= 1 + \frac{d(\ln R)}{d(\ln \Phi)}\bigg|_{\Phi=\Phi_0} \ln(\Phi/\Phi_0) + \cdots. \quad (8)$$

We define the quantity

$$\gamma^* \equiv (\ln 10) \frac{d(\ln R)}{d(\ln \Phi)}\bigg|_{\Phi=\Phi_0}. \quad (9)$$

This is a generalized contrast parameter which in the case of photoresists operating at $\Phi_0 = E_0$ (Fig. 5) becomes $\gamma^* = \gamma$. For photoresists, $R(\Phi)$ is the amount of resist removed following standard development. In general, γ represents on a semilogarithmic scale, the sensitivity of the laser-induced rate to *incremental* variations in fluence. As with the traditionally defined quantity, γ^* may be a function of the operating fluence, although in practice it is frequently constant over a wide range.

Photoresists are generally assumed (correctly) to be reciprocal, that is, to have linear dependence on intensity (i.e., dose rate). As a result resist exposure can usually be expressed unambiguously in energy density (mJ/cm^2), that is, the product of intensity and exposure time, without specifying intensity level of the exposure. For excimer systems, this

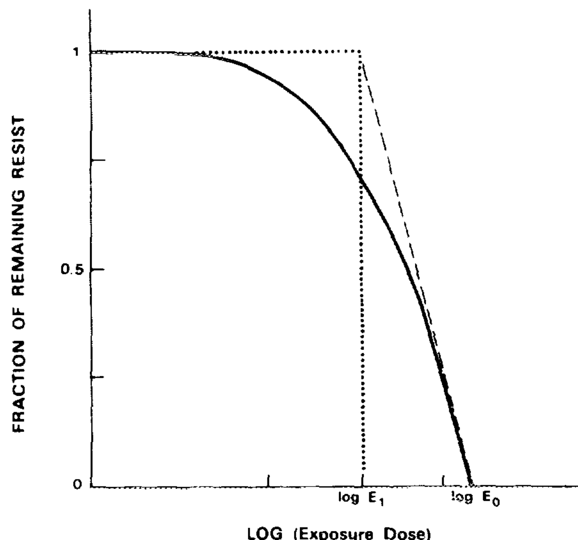

FIG. 5. Characteristic exposure curve for a positive photoresist. The ordinate is the fractional thickness of resist remaining after development. The dose E_0 is the threshold exposure. The value of γ is determined by the slope of this curve at E_0, $\gamma = [\log_{10}(E_0/E_1)]^{-1}$.

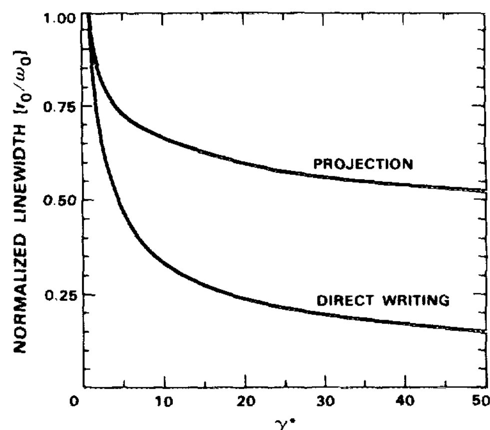

FIG. 6. The calculated resolvable linewidth as a function of γ^* for the two patterning configurations, direct writing and projection. In this model the smallest separation $2r_0$ between two parallel exposed lines was determined. The lateral extent of the fluence distribution of each exposed line was taken to be constant: $\Phi(r) = \Phi_0 \exp(-2r^2/\omega_0^2)$, and the smallest resolvable separation was calculated so that the photoinduced process rate $R(\Phi)$ [Eq. (8) in text] vanishes midway between the lines, at $r = r_0$. In direct writing the rates due to each line are added, whereas in projection the fluences are summed first. This geometry should be contrasted with that of equal lines and spaces, which is commonly used in calculating the MTF (Fig. 3).

simplification often breaks down. However, such nonreciprocal responses are generally of the opposite sign to the nonreciprocity of photographic film and, in general, are beneficial for image recording. It has been pointed out previously[26] that nonreciprocity of the positive sign, that most frequently encountered in laser reactions, is a powerful benefit in direct writing (scanned, focused-beam reactions). For dense patterning, a 4× reduction in linewidth (resolution improvement) beyond that attributable to high contrast (large γ) alone is frequently obtained. In projection printing this *explicit* benefit from nonreciprocity is not present; however, the high contrast it can imply is beneficial at least to a point.

The case of patterning of fixed-width lines and variable spaces as predicted by simple two-dimensional patterning theory[26] is illustrated in Fig. 6. Note that for this case, resolution for projection printing improves with increasing γ^* up to a value of ~ 10, well beyond that obtained with wet-developed conventional resists. Unlike laser direct writing, however, there is very limited resolution advantage (and only increased process criticality) for greater values. Since the case modeled in Fig. 6 is typical in practice, we conclude that excimer patterning processes are optimally tuned for $\gamma^* \approx 6$–15. This is frequently possible by adjusting resist properties or gas ambients. Unlike traditional resists, nonlinearities in laser reactions are frequently actually detuned in order to lower values of γ^*.

In the sections below we discuss the three main classes of excimer laser projection imaging materials. The first of these, the injected defect system, is the category which includes almost all existing organic and inorganic optical photoresists exposed by lamps. These systems have prevailed with lamp exposure because radiation-induced defects can have strong effects on film dissolution (development), and therefore provide high sensitivity (high gain) for low-intensity radiation. High-peak-power and short-wavelength excimer radiation permits comparable sensitivity in two additional classes of systems. These are the solid transformation systems, including the ablative resists, and the interfacial reaction systems. Similar sensitivity to that of current lamp resists can be obtained for both of these, but only indirectly in the last class. As mentioned above, ablative (self-developing) systems can significantly simplify lithography sequences. The last class contains systems which pattern wafers directly and therefore may have unique applications in resistless processing. Tables I–III list the material systems demonstrated in excimer projection at the time of this writing. We have attempted to be complete in these listings. In addition, Table IV shows several excimer contact printing experiments. We note that these last results may or may not be directly transferable to projection; we include them largely for the data they provide on the sensitivity of material responses.

Finally we make a specific comment on single-pulse (typically 20 ns) exposure, which can be achieved in some systems. Single-pulse exposure has potentially distinct advantages for applications with step-and-repeat systems. For example, the presently stringent requirements for mechanical stability of the projection system and the processing-time overhead needed for table settling could possibly be significantly relaxed by using an exposure "on-the-fly" strategy. The full utilization of the unique capabilities of single-pulse exposure requires considerable, but achievable improvement in the pulse-to-pulse energy stability of excimer lasers.[27]

B. Injected-defect responses

To obtain sensitivity (or gain), lamp-based photoresists are generally based on localized modification of organic or inorganic films by photoinjection of defects, such as by bond scission (for positive resists) or crosslinking (negative resists). In these traditional photoresists, defects are generated via single-photon electronic transitions. Clearly, in their spectral range of optimization, established resists can be exposed with excimer radiation, and performance comparable to lamp exposure can be obtained. Work to extend these traditional systems into the deep UV is only beginning. The work published to date is listed in Tables I and IV. At least

TABLE I. Injected defects (projection).

	Laser wavelength (nm)	Dose/pulse (mJ/cm^2)	Total dose (mJ/cm^2)	Resolution (μm)	Reference
1. Organic resists					
(Wet developed)					
Diazonaphthoquinone—Novolak	308	5	100	1	61
MP 2400					
	248	0.01–10	80–200	0.4–0.5	8, 9, 11
PMGI	248	40	10 000	0.30	10
PMMA	248	17	32 000	0.35	10, 11
PMMA	193	1000	1000	0.13	50
2. Doping					
Si/BCl_3	193			0.5	13

TABLE II. Ablation and solid transformation (projection).

	Laser wavelength (nm)	Dose/pulse (mJ/cm^2)	Rate (nm/pulse)	Resolution (μm)	Reference
1. Organics					
Diazonaphthoquinone/ Novolak resist	193	18	20	2	41
Polyimide	193	18–3000	20–300	0.9–2	41, 42, 50
AZ 1350 J resist	193	80	140	0.4	13
PET	248, 308	180–250	190	19	62
PMMA	193	1200	150	0.3	50
2. Inorganics					
Aluminum	308	140–700	50–80	5–30	44, 46
Gold	193	1000	100	5	45
Pyrex	193	500	150	0.4	13
Al/O cermet	193	130	30	< 1	13
Au resinate	248	5	0.3	1	47
Pt resinate	248	5	50	1	47
InP	193	100	0.3	2.5	50
GaAs	193	20	0.025	4	49
Diamond	193	65 000	140	0.13	48
Diamondlike carbon resist	193	130	200	0.13	3

for several of these, it has been shown[28,29] that traditional resist responses remain reciprocal up to flux levels on the order of 5 MW/cm^2. For other systems positive nonreciprocity is readily obtained, although its generality is unknown. Table IV lists a result obtained in the $GeSe_x$ inorganic resist[30] where strong positive nonreciprocity occurs and increases the sensitivity of this material by a factor of 25, to make it quite comparable in response to the best optical (lamp) resists. The mechanisms of positive nonreciprocity are not well established.

In the spectral range of greatest interest ($\lambda < 300$ nm), very few properly designed traditional resists have yet been reported. Extensive testing was performed on Novolak-resin-based, visible/near-UV lamp resists, at short wavelengths. Most of these were found to be much too strongly absorbing for good profile control. Furthermore, the absorption does not exhibit photobleaching, often leading to even more sloped profiles.[31] The photoabsorption at 248 nm apparently leads to crosslinking in the resin, which manifests itself as a 2–5 times reduced development rate, following exposure and a postexposure bake.[32] Only the AZ 2415 and MP 2400-17 were transparent enough to be used at 248 nm. Indeed, excellent results down to 0.35-μm lines have been reported[8-11] with projection patterning of MP 2400 and the newly developed resist PMGI (see Figs. 7 and 8). Exposure doses were ~ 100 mJ/cm^2 for ~0.5-μm-thick films. A number of new resists have been reported for the deep UV, including organosilicon resists,[33] and copolymers and terpo-

TABLE III. Interfacial reactions (projection).

	Laser wavelength (nm)	Dose/pulse (mJ/cm^2)	Rate (nm/pulse)	Resolution (μm)	Reference
1. Driven systems					
Deposition					
Cr[from $Cr(CO)_6$]	248			10	52
Au[from $Me_2Au(acac)$]	193, 248, 308	618	0.2	2	53
Au[from $Me_2Au(hfacac)$]	248	60	0.013	1.6	50
2. Surface modification					
(a) Etching					
Mo(with Cl_2)	193	1–10	...	10	50
(b) Deposition					
Al(from TMA, TIBA)	193, 248	1–30	...	2–5	54, 56, 59
(c) Polymerization					
Polyethylene (catalyst from TMA & $TiCl_4$)	193	1–10	...	3	57

TABLE IV. Other material systems (contact printing).

Material	Wavelength (nm)	Total dose (mJ/cm^2)	Development conditions	Film thickness (μm)	Resolution (μm)	Reference
1. Inject defects (Wet developed)						
PMMA	200–260		MIBK, 2 min	1.2	<0.5	63
	193	45 000	40:60 MIBK:IPA 2 min	0.05	0.05	64
PMIPK	215–300		ODUR developer, 1 min	0.5	0.5	65
Meldrum's diazo sensitizer/cresol novolac resin	254	50	1:3 AZ developer: H_2O 4 min	1		31
Sensitized para-cresol resin	254	15	1:3 AZ developer: H_2O	1	2.7	66
P(MAN-co-MAC)	254	50	1:5 H_2O:EtOH 5 min		1.5	67
$Ag_2Se/GeSe_2$	248	5.2–130		0.18	0.5	30
AZ 2400	248	180	1:4 AZ 2401:H_2O 1 min	1	1	29
Sensitized maleimide styrene copolymers	280	50		0.9	~ 1	62
AZ 2415	248	100	1:4 AZ 400K:H_2O 2 min	0.5	0.5	34
P(MMA-co-MMA) + 20% *o*-nitrobenzyl cholate	248	120–180	2.5% diethanolamine in H_2O 10 s	1	>1	34
P(MMA-co-IN)	248	450	MIBK, 1–2 min	0.47	1	34
P(MMA-co-OBM)	248	1000	60:40 MIBK:IPA 1 min	0.54	0.75	34
P(MMA-co-OBM-co-MAN)	248	350	60:40 MIBK:IPA 1 min	0.48		34
2. Ablation/solid transformation						
Nitrocellulose	193	500	...	1	1.9	40
PMIPK	193	1000	...	1	0.5	36
AZ 2400	193	1000	...	1	0.3	36
PMMA	193	1000	...	1	0.5	36

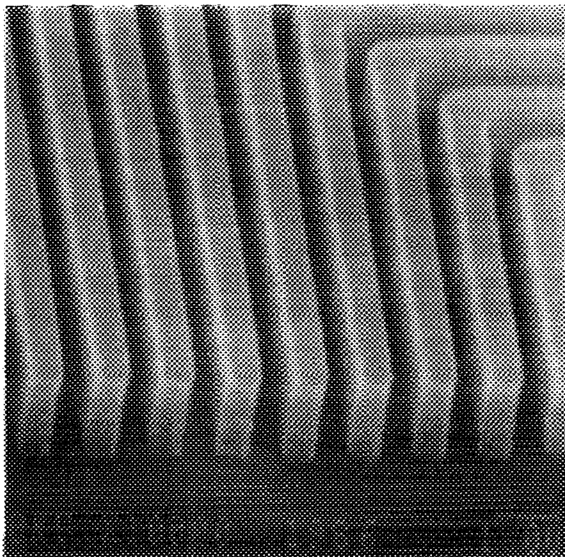

FIG. 7. Scanning electron micrograph of 0.5-μm lines and spaces, obtained by excimer projection patterning of a trilevel, with MP 2400-17 as the photoresist (imaging layer). Exposure was at 248 nm, with 0.6 mJ cm^{-2} pulse^{-1} fluence, and total dose of 0.12 J cm^{-2} (from Ref. 8(b), courtesy of V. Pol and G. C. Escher, reprinted by permission of SPIE).

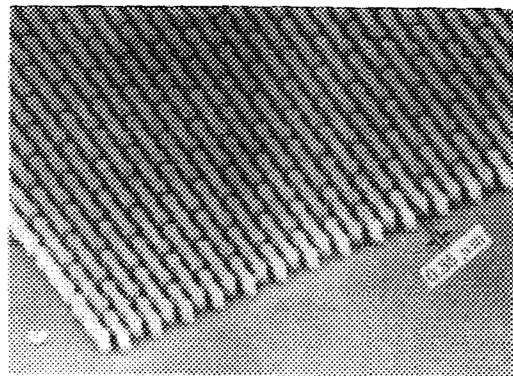

FIG. 8. Scanning electron micrograph of structures with 0.35-μm resolution, obtained by excimer projection patterning of a trilevel, with PMMA as the photoresist. Exposure was at 248 nm, with 17 mJ cm^{-2} pulse^{-1} fluence, and total dose of 32 J cm^{-2}. Shown are the structures after reactive ion etching of the planarizing layer (from Ref. 10, courtesy of Y. Horiike, reprinted by permission of SPIE).

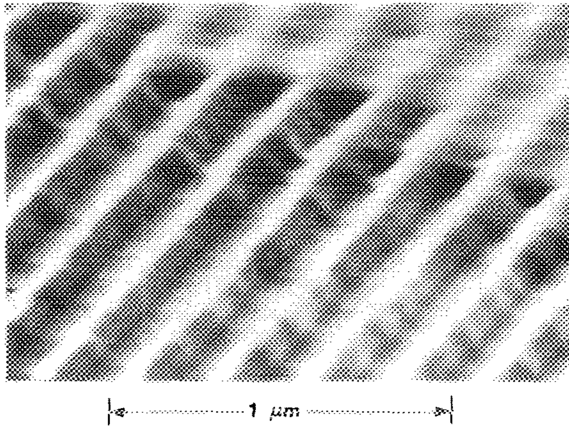

FIG. 9. Scanning electron micrograph of nominal 0.13-μm lines and spaces etched in 150-nm-thick PMMA on Si. Exposure was with one pulse from an excimer laser at 193 nm (~ 1 J/cm^2), and development was for 5 min in a 60:40 solution of methyl isobutylketone:isopropyl alchohol.

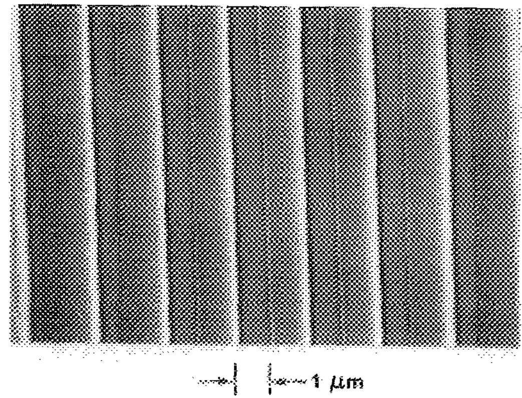

FIG. 10. Scanning electron micrograph of projection-etched 1-μm-thick polyimide on oxidized silicon. The 0.9-μm lines and spaces were obtained with 10 pulses of 1 J cm^{-2}/pulse at 193 nm. Exposure was in air.

lymers of polymethyl methacrylate (PMMA).[34] Figure 9 shows a high-resolution result from our own laboratory utilizing wet-developed PMMA. We obtained 0.13-μm lines and spaces using one 193-nm pulse.

A further type of nonconventional injected-defect response can be obtained by excimer-laser doping of inorganic materials. The exploration of these processes is at early stages. The principle of operation is to drive minute amounts of impurities into inorganic thin films, thereby changing their solubility or dry-etch resistance. A substantial gain can be achieved; for example, 1 part impurity in 10^4 injected into a semiconductor can change its dissolution (development) rate in etchants by many orders of magnitude. Typically doping is by diffusion or phase transition and can have a strongly nonreciprocal response, allowing also large γ^* ($\gamma^* \approx 40$). Early results in boron doping of silicon were reported in Ref. 13. The $AgSe_x$ resists[30] may also be considered as belonging to this category. In cases where the transport properties of the bulk resist matrix are affected in a transient fashion by pulsed excimer radiation, injected-defect responses are sometimes enhanced by solid transformation responses as discussed below.

It is expected that the optimization of injected-defect organic resists will be relatively rapid; however, these systems may well be supplanted nearly simultaneously by the powerful solid transformation resists discussed below.

C. Ablation and solid transformation responses

1. General

A second category of systems respond by laser-induced nonlinear homogeneous transformations. These are extremely promising although unconventional resist systems, which may well become the dominant excimer stepper lithographic materials. All make explicit use of the higher dose rate possible with lasers relative to lamps. It is notable that the dose requirements for favorable systems in this category can be comparable even at this early state of development to injected-defect photoresists for the visible. All the systems discussed below make more efficient use of deep-UV photons than does wet-developed PMMA. Many have highly superior processing properties and are self-developing.

2. Organic systems

Perhaps because of their existing well-established uses as resists, organic films are also among the most widely explored of the solid-transformation systems. Studies have concentrated on ablation which results in a self-developing response. The first experiments, carried out in a contact printing geometry, were those of Srinivasan and Mayne–Banton who studied principally polyethylene terephthalate (PET) films.[35] This work stimulated a great deal of interest, particularly as the mechanism of ablation was shown to be complex and, among other things, strongly wavelength dependent. Several groups have studied these systems in some detail.[36–39] Nitrocellulose films have also been examined.[40] The extension from contact printing to high-resolution projection printing in such organic single layers is not necessarily trivial.[41] However, our own experiments have demonstrated that clean 0.9-μm lines and spaces can be obtained in 1-μm-thick polyimide films (see Fig. 10). Exposure is by direct ablation with 1–10 pulses of 193-nm radiation at fluences $\sim 10^2$–10^3 mJ/cm^2. Polyimide is also a useful dielectric for separation of multilevel metallizations. The same self-developing process has been applied to excimer projection etching of interlevel vias[42] with no further processing or cleanup for good contact formation (see Fig. 11).

Significantly higher resolution was obtained in the original projection etching experiments[13] by use of organic bilayers. Two-layer spin-on systems very similar to those developed for lamp exposure[43] were employed. A modified method of use, in which the top layer is reactively removed by 157- or 193-nm irradiation, has permitted single-pulse printing of 0.2-μm lines and spaces. The bilayer is formed by overcoating a 1.5-μm-thick soft-baked PMMA layer with several UV absorption lengths of AZ 1350J resist. The top

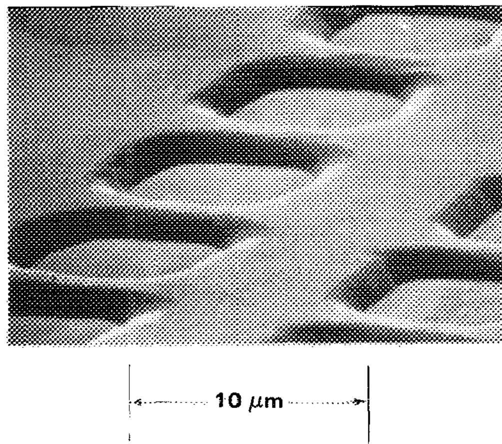

FIG. 11. Scanning electron micrograph of via holes in 1-μm-thick polyimide on oxidized silicon. The pattern of 6-μm holes was etched in projection with five pulses, 3 J cm^{-2}/pulse, at 193 nm. Exposure was in air.

layer is removed by ablation with a single pulse without disrupting the underlying PMMA. The image is then developed using UV flood exposure and wet etching in isopropanol/methyl isobutylketone.

A primary advantage of the bilayer is that thin AZ-resist imaging layers can be used. Importantly, a thin contamination or remnant of this layer often left in unoptimized lamp exposure does not interfere with clean development to the substrate surface. Nominal 0.4-m lines and spaces in 1.5-μm-thick PMMA (aspect ratio ~4) and 0.2-μm lines on 0.8-μm centers are shown in Fig. 12 (note that this last structure has an aspect ratio >8 to 1). Both were produced using single pulses of 193-nm radiation; comparable results, but without significant improvement within our limited optimization, were observed with 157-nm (F_2-laser) radiation. The highly nonlinear intensity response of the overlayer to ablation produces high resolution and sharply defined edges. The required single-pulse fluence is ~80 mJ/cm^2 at 193 nm.

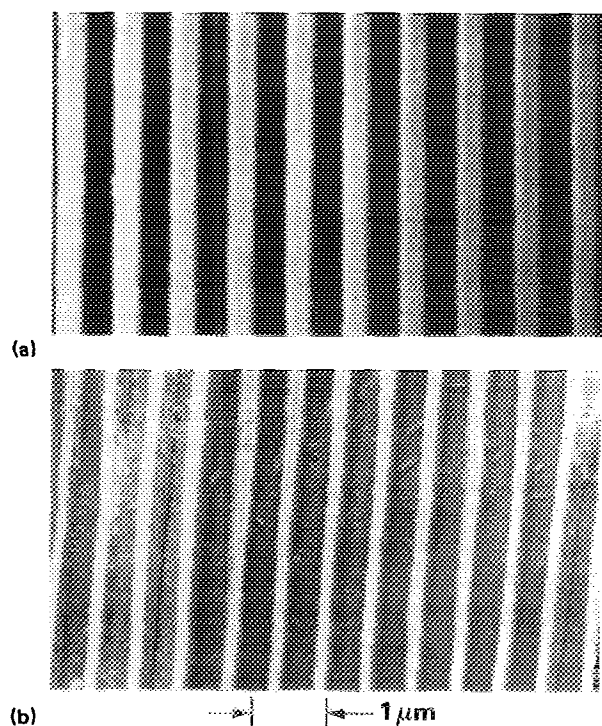

FIG. 12. Projection patterning of an organic bilayer. A 140-nm-thick film of AZ 1350 J, which served as the imaging layer, was ablated in one pulse (80 mJ/cm^2) of 193-nm radiation. The underlying planarizing layer was 1.5-μm-thick PMMA. Following patterning of the imaging layer, the PMMA was exposed to UV-lamp flood illumination and the exposed areas were wet developed. The figures are scanning electron micrographs of (a) 0.4-μm lines and spaces, and (b) 0.2-μm lines on 0.8-μm centers. Note that the aspect ratio of the smaller 0.2-μm lines exceeds eight. Some damage is done to the fragile structure by the heavy electron dose used in scanning electron microscopy.

3. "Diamondlike" carbon resist

The highest resolution yet obtained by excimer projection is with the hard diamondlike carbon resists exposed by single 20-ns-ArF laser pulses in a self-developing response.[3] These materials are low-hydrogen-content carbon films that have better dry-etch resistances, and therefore utility at smaller thicknesses, than typical organic materials. Thin resist films of 100- to 200-nm thickness are applied by rf plasma deposition from butane (rather than spin-on) and exposed with excimer pulses of 0.1 to 1 J/cm^2.

Figure 13 shows a scanning electron micrograph of 0.13-μm lines and spaces patterned by 193-nm laser projection onto hard carbon resist on GaAs. The fluence, ~0.13 J/cm^2, was near threshold for ablation, and its effect was "blistering" of the carbon, which is nevertheless sufficient for subsequent preferential dry etching of the GaAs substrate with excellent edge definition. Resist removal is by O_2 plasma.

We note the high optimization of this last system. The 0.13-μm-wide lines are significantly smaller than the wavelength of the laser and, in fact, approach the absolute diffraction-limited cutoff width, $\lambda/4$ NA = 0.097 μm for the 0.5-NA optics. Key to the excellent performance are single-pulse exposure, a high contrast response ($\gamma^* \approx 22$), and built-in "bleaching" via saturation of the resist response at high exposure.

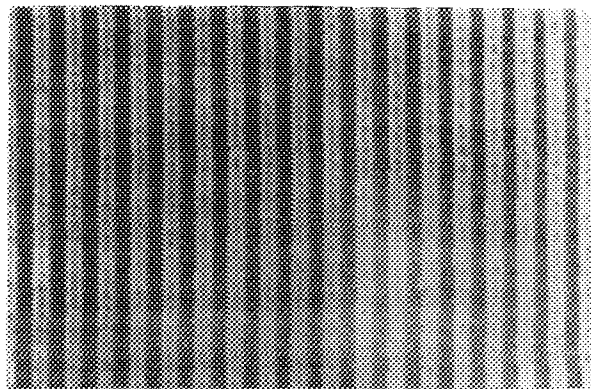

FIG. 13. Scanning electron micrograph of 0.13-μm lines and spaces, patterned in hard carbon film on GaAs. The film thickness is 100 nm, and the projection patterning was performed with one 193-nm pulse (130 mJ/cm^2) in air.

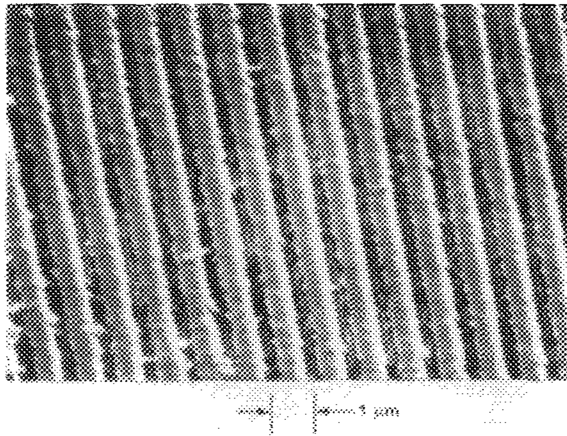

FIG. 14. Scanning electron micrograph of nominal 0.4-μm lines and spaces, etched in Pyrex in projection. Exposure conditions were three pulses at 193 nm at 0.8 J cm^{-2}/pulse, in a 200-Torr H_2 ambient.

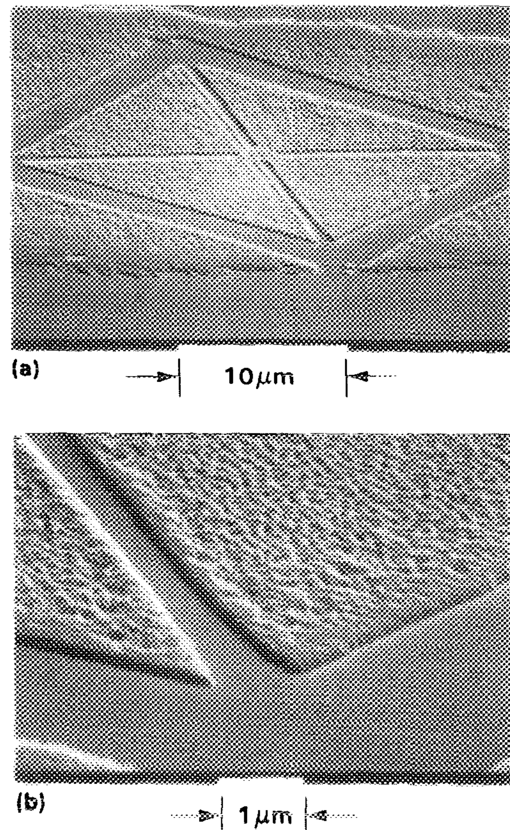

FIG. 15. Scanning electron micrographs demonstrating the excellent submicrometer resolution obtainable in projection patterning of an Al/O cermet film at 193 nm. One 120-mJ/cm^2 pulse was used to induce solid-state transformations in the 30-nm-thick film. Development was performed by wet etching in nitric-acid/phosphoric-acid followed by reactive ion etching in CHF_3.

4. Metal and dielectric films

Existing trilevel lamp resists frequently employ thin metal or dielectric layers for their dry etch resistance which is unparalleled in organics. Direct patterning is possible with an excimer laser. Andrew *et al.*[44] have studied single-pulse ablation in air of several metals including Ni and Cr with a 308-nm XeCl laser. Threshold exposures for 100-nm-thick films on glass are 0.2 J/cm^2. Other systems studied,[45] sometimes with chemical enhancement include W, Mo, and Au. A combined chemical/ablative process for etching of Al was applied to projection etching of 5-μm-diameter via holes by Koren *et al.*[46] Submicrometer spatial resolution has yet to be demonstrated in these systems.

Less work has been reported in inorganic dielectric systems. Ehrlich *et al.*[13] demonstrated projection etching of 0.4-μm lines and spaces in Pyrex using a H_2 ambient. The reaction has high contrast and natural bleaching as indicated in Fig. 14. The process is extendable to other absorbing glasses.

5. Thin film solid-state chemistry

In principle, a large variety of transformations can be induced by laser irradiation of metastable solid films. The materials studied to date include spin-on organometallic resonate complexes and evaporated Al/O cermets. These systems and other metal/dielectric composites are particularly interesting since both chemical (e.g., etch resistance) and electrical properties can be altered with excimer pulses. This suggests potential direct applications as electronic device materials.

The best lithographic performance has been achieved in the cermets.[13] In these studies, a 30-nm-thick Al/O cermet was deposited by Al evaporation under an O_2 ambient at $2-5\times10^{-6}$ Torr O_2 pressures. As evaporated, these films have a sheet resistance of 1000 $\Omega/\Box$, and are smooth and shiny in appearance. The conversion process proceeds through several stages which correlate with visible color changes. The mechanisms of transformation are discussed in Ref. 13. A large (more than a 1000-fold) conductivity change induced by excimer pulses in these cermets is of potential use for defining conductor patterns without any further treatment.

Alternatively, the transformed material can be used as an etch mask to pattern underlying materials. To demonstrate the second application, images were transferred into SiO_2 by wet etching in nitric-acid/phosphoric-acid followed by reactive ion etching in CHF_3. Typical results obtained with single-pulse excimer laser exposure are shown in Fig. 15.

The other solid-state chemical systems, namely, the organometallic resonates, are commercially available spin-on materials with typical metal content of 20%–30%. Houlding *et al.*[47] have demonstrated that these materials (Au and Pt complexes) have a photochemical negative-acting response at 248 nm or, alternatively, can be ablated at high ($\sim$1 J/cm^2) fluence. Development of the photochemical response is in a hexane wash. Projection patterning on a $\sim$1-μm scale was obtained with these systems.

6. Direct substrate etching by heat/chemical pulse

Direct etching of various semiconductor substrates has been demonstrated for a number of materials. Although all of these systems utilize a controlled (typically oxygen- or halogen-containing) ambient and therefore have mechanistic analogs in the interfacial chemical systems in Sec. III D

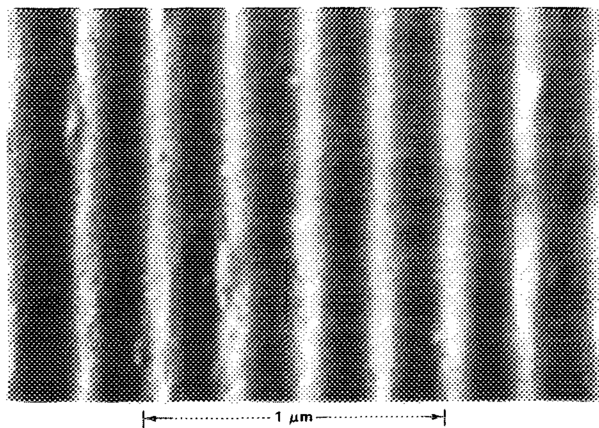

FIG. 16. Scanning electron micrograph of a 0.25-μm-period grating etched in crystalline diamond with a 193-nm laser. The ~100-nm-deep grating was generated in projection with one pulse (65 J/cm^2) in air.

below, all have been reported to operate best in the regime of significant pulsed heating/ablation. Resolution is largely defined by the lateral extent of the heat pulse. We therefore consider them, somewhat arbitrarily, as transformation systems.

The highest resolution among these systems is achieved in etching diamond.[48] The ArF laser, at 193-nm wavelength, is particularly suitable for this interaction, since the photon energy at this wavelength (6.4 eV) is higher than the band gap of diamond (5.4 eV). Etching is under Cl_2, O_2, or NO_2 ambients. Well-defined gratings ~100-nm deep with *periods* as small as 0.25 μm were obtained in single, 15-ns-long pulses. An example is shown in Fig. 16. For such single-shot exposures, nearly sinusoidal features with an amplitude close to the half-period (i.e., linewidth) dimension are achieved.

As described in Ref. 48, two processes take place during laser irradiation: conversion of diamond to graphite and sublimation or reaction of carbon. To reduce the required temperature and eliminate accumulation of graphite, ambient vapors are used to react with the heated graphitic layer. Volatile products (CCl_4, CO, CO_2) are formed at temperatures below sublimation, and the amount of graphitic residue is reduced dramatically. The best results were obtained with gases simultaneously photolyzed during the pulse. Under typical conditions, free radical densities of 10^{17}–10^{18} cm^{-3} are generated by the laser near the surface. Based on our observations, these radicals react with near unit efficiency with the hot graphitic layer. More on the mechanism can be found in Ref. 48.

Other semiconductor substrates etched in projection include III–V materials under conditions approaching ablation. Brewer *et al.*[49] have demonstrated etching of GaAs at 193 nm. The process is initiated by the vapor-phase photolysis of HBr. Linewidths of 4 μm were achieved with 0.5-Torr HBr in 10-Torr buffer gas (Ar or H_2). The etch rate was ~0.25 Å/pulse at a fluence of 20 mJ cm^{-2}/pulse. In our own experiments,[50] another III–V compound, InP, has been etched in projection with 1-Torr Cl_2 and no buffer gas. The laser, operated at 193 nm and 20-Hz pulse repetition rate, induced etch rates of ~3 Å/pulse at fluences of 100 mJ cm^{-2}/pulse. The resolution was ~2.5 μm. In both instances the etching process is initiated by photolysis of the halogen-containing molecule (HBr or Cl_2) and generation of a high density of reactive halogen atoms (Br or Cl, respectively). These in turn react with the surface, leading to volatile halide molecules. Thus the overall chemical process can be represented in the form:

$$X(s) + 3Y(\text{vapor}) \rightarrow XY_3(\text{vapor}),$$

where $X(s)$ is a surface atom (Ga or As for GaAs, In or P for InP), and Y(vapor) is the photogenerated halogen atom (Br or Cl). Further experiments on InP etching have been carried out by Aylett and Haigh.[51]

D. Interfacial chemical and surface modification responses

1. General

This category includes the majority of resistless laser-driven photochemical etching and deposition reactions. The practical realization of these reactions is seen as more distant than excimer processing with resists, but the leverage in processing simplification is great. The essential feature of these responses is the interaction between the laser light and some external-phase (vapor-phase or adsorbed) species, and the subsequent reaction between the products of this interaction and the surface. Naturally, the laser may at the same time interact with the solid phase as well. These processes are limited fundamentally by the material coverage of an adsorbate, or by surface-collision frequencies from the external phase. For the case of substrate/adsorbate reactions at modest (> 100 mTorr) pressures, the adsorbate coverage can be assumed to have reached equilibrium between laser pulses. The maximum reacted thickness per pulse is then approximately equal to the adlayer thickness itself. The actual reacted thickness per pulse is typically less. Similarly, for the case of substrate/gas-phase reactions at subatmospheric pressures, the reacted thickness per pulse is limited to the gas exposure per pulse. For 8–30-ns pulsewidths and subatmospheric pressures, this is ~1 langmuir. As a result of these limitations on reacted thickness per pulse, the low duty factor (~10^{-5}) of current excimer lasers implies long exposure times even for efficient chemical systems.

Furthermore, for the case of substrate/gas-phase reactions, the resolution may be limited by lateral diffusion of the photogenerated species. This effect can be reduced by the addition of buffer gases, usually at the cost, however, of a reduction in the overall reaction rate. As a result of these considerations the rates and resolution thus far achieved in photochemical projection etching and deposition have been significantly lower than those of the transformation systems detailed in the previous section. An important way to circumvent these limitations is via laser-induced surface modifications (e.g., of single monolayers) which are subsequently "chemically amplified" by nonlaser reactions. We first discuss continuously driven reactions, then the surface modification systems.

2. Photochemical continuously driven reactions

The high-resolution, high-rate laser deposition of materials by projection is a difficult problem. Experiments to date have concentrated on metal deposition in the regime of thermally accelerated photodeposition, i.e., conditions where the excimer pulse heats the deposited film to achieve a thermal (pyrolytic) rate component which supplements molecular photolysis. The thermal component is difficult to control. Early experiments were carried out by Yokoyama *et al.*[52] on deposition from $Cr(CO)_6$. Thick Cr-containing films with several-micrometer features were obtained using 248-nm fluences of several hundred mJ cm^{-2}. Aylett and Haigh,[51] and Baum *et al.*[53] achieved similar results for gold from trimethylgold–trimethylphosphine and dimethylgold–acetylacetonate derivatives, respectively. Tsao and Ehrlich[54] deposited Al films from triisobutylaluminum. By use of the thermally accelerated photodeposition mechanism, rates on the order 1 Å/pulse have been possible in good systems. With an excimer laser operating at 10^2–10^3 Hz, acceptable processing throughput appears possible. Submicrometer resolution and electronic-quality material properties have yet to be demonstrated.

As discussed above in Sec. III C 6, a number of etching reactions are a combination of interfacial-chemical and solid-transformation processes, with the solid-transformation (typically product vaporization) dominating as resolution determining. Further etching reactions for refractory metals, Si, and Si_3N_4 have been developed by Loper and Tabat[55] using photolysis of COF_2 and NF_3. These last examples were pursued to low (< 100 mJ/cm^2) fluence where the patterning resolution is presumably determined by gas-phase or surface recombination kinetics of the active radicals.

3. Surface modification reactions

Finally, we briefly discuss a special subclass of interfacial chemical responses which have important, longer range potential. These are applied to patterning of more or less conventional vapor deposition or etching processes but achieve higher photon efficiencies, therefore lower dose requirements, than the continuously driven reactions of the previous section. This efficiency is via process gain, i.e., greater than unity absorbed-photon efficiency. Somewhat like usual photoresist processes where gain is obtained during solvent development, laser surface modification processes achieve gain also by chemical amplification. However, unlike photoresists the radiation effect is by the alteration of the first monolayers of the substrate surface rather than the injection of defects into a bulk film. These first monolayers often control surface reactivity or nucleation of new phases at the substrate/vapor interface. At the time of this writing powerful chemical effects have been discovered, many in laser writing experiments; none has yet been demonstrated at highly submicrometer linewidths. However, there appears to be no fundamental reason that high resolution will not be achieved.

Although perhaps feasible earlier (with lamps), surface modification patterning has only now come under development with the use of highly "actinic" photons from excimers. Since surface modification processes are new to microfabrication, and their essential motivation relies on their efficiency, some words are merited on the estimation of theoretically obtainable gain. For these material systems, gain is a statistically defined parameter depending directly on the patterned area (wafer size). Obviously it also depends on the heterogeneous surface kinetics of the reactions, therefore on surface composition, growth rate, temperature, etc. We first make a few general remarks about the efficacy of surface modifications, then summarize the work to date.

a. Theoretical gain for surface modifications. A qualitative treatment for growth by laser surface modifications has been presented previously.[56] A similar model will apply for etching. In this treatment the laser-induced lowering of two types of growth barrier is considered in terms of a figure of merit, defined as the ratio of growth to nucleation rates. This figure of merit has the units of volume. Theoretical gain is obtained by dividing it by the volume of a monolayer surface coverage (or, more generally, the volume of the active modifier) on the wafer surface. The first type of barrier is derived from surface tension, which impedes the nucleation of physical phase changes such as condensation. Such barriers are due to the critical balance between surface and volume contributions to the free energy of transformation. In these cases, laser irradiation can be used to deposit films which act as surfactants, lowering or eliminating the initial condensation barrier. In the later stages, the deposit acts as its own surfactant, sustaining further growth.

The second type of barrier derives from surface-catalysis effects which impede the nucleation of chemical changes by surface reactions. This class of processes has been used widely (e.g., tungsten deposition without lasers) for selective chemical vapor deposition (CVD) on photolithographically patterned surfaces. To intervene in these cases the laser deposits a pattern of heterogeneous catalyst to initiate a transformation that is chemically self-sustaining, or autocatalytic. Reference 56 treats these two classes of systems according to simple kinetic considerations. The theoretical area $\times$ height figure of merit Ah for extended area defect-free patterning is plotted versus the required laser-induced free energy change for the two cases in Figs. 17 (a) and 17(b). In each the parameter regime for a gain of 10^3 is

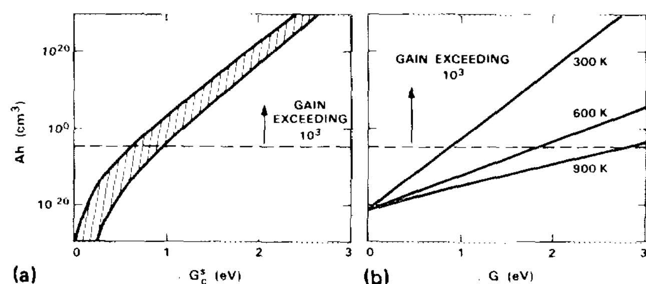

FIG. 17. The figure of merit Ah for laser surface barriers. (a) As a function of the critical free-energy barrier for physical surface nucleation ΔG^*_c. The two solid lines represent metal deposition on a dielectric in the limit of low vapor pressure (upper curve) and high vapor pressure (lower curve). The shaded region corresponds to intermediate pressures. (b) As a function of the total free-energy barrier ΔG for chemical nucleation, for three temperatures. The figure of merit has a very steep dependence on ΔG at room temperature and a weaker dependence at elevated temperatures.

indicated . This value is typical of good photoresists, over a 82 cm^2 wafer. This is the parameter regime for practically useful full-wafer patterning by processes of these generic classes. More details of the analysis are found in Ref. 56. We next discuss a few specific examples. The three processes discussed all operate dominantly through barriers of the second type.

b. Monolayer catalysts for addition polymerization. One particularly efficient laser-nucleated chemical process that has been demonstrated is monolayer catalysis of polymerization of unsaturated hydrocarbons.[57] This procedure can be varied to pattern vapor-phase growth of a wide variety of organic films—in somewhat the reverse of usual resist processing. Exceptional step coverage can be achieved. The initiation of polymerization in the pure hydrocarbon is normally difficult, because of the necessity of free-radical formation. The laser intervenes in the initiation by depositing patterned thin films of polymerization catalyst.

The laser-deposited film, in the best characterized case discovered so far, is a compound photodeposited from mixtures of $TiCl_4$ and trimethylaluminum (TMA). As discussed elsewhere,[58] the overall reaction for photodeposition from these molecules has the characteristics of a chain reaction in the mixed-component adsorbed layer. The most important features can be understood by a simple model in which the reaction is initiated by the sequence of parent-molecule adsorption and photoreaction to form a surface complex.

Separate experiments have demonstrated that this complex is apparently chemically very similar to Ziegler–Natta catalysts, in that it acts as an efficient catalyst for room-temperature chain polymerization of unsaturated hydrocarbon vapors.[57] The low temperature of the reaction suppresses any appreciable background polymerization. The energetics put many common organic systems well into the useful region in Fig. 17(b).

c. Photonucleated chemical vapor deposition. A similar process has been demonstrated[56] for Al CVD. The basic experimental result is shown in Fig. 18 and described in the caption. The maximum growth thickness possible before background nucleation becomes significant was not studied in detail. However, under conditions similar to those used for Fig. 18 nonphotonucleated growth did not occur for a period, implying that over 1-μm-thick films can be grown without background nucleation. Separate measurements have shown that photodeposition of several monolayers is sufficient to achieve selective CVD with triisobutylaluminum (TIBA). This same reaction in TIBA has recently been applied[59] in the metallization of field-effect transistors in a KrF-laser-based projection geometry. A resistance of 1 Ω was achieved for gates 6 μm wide and 1 μm thick. Photoinhibited CVD of aluminum by photodeposition from trimethyaluminum, by a possibly similar process, has also been demonstrated.[56]

d. Halogenation for etching of refractory metals. As a final example, thin films of Mo and W have been etched in a two-step process, where the projection patterning takes place in the first surface modification stage.[50] The surface modification consists of a laser-induced chemical change in the first monolayers of the film in the presence of a Cl_2 ambient. The 4- to 5-nm-thick native metal oxide is removed with 193-nm pulses and is replaced with a metal chloride layer. This surface pattern is then amplified by etching through the metal film with NF_3 under conditions of broad-area heating. The native oxide is resistant towards etching with NF_3, and therefore selective etching of the prehalogenated areas is achieved.[60]

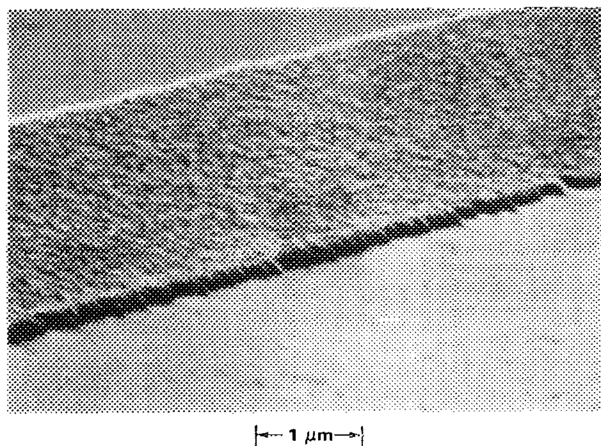

FIG. 18. Photonucleated CVD of aluminum stripe. A 257.2-nm UV laser beam, generated by frequency doubling the output of an Ar^+ laser beam, first photodeposited a ~5-nm-thick stripe onto a quartz substrate in a saturated vapor of triisobutylaluminum (TIBA). The UV laser beam is then switched off and a CO_2 laser beam is shuttered on. The CO_2 laser radiation is absorbed strongly by the quartz and acts only as a convenient, modestly localized heat source for thermal CVD. After a 2-min exposure to the CO_2 laser beam, no CVD occurs on the bare quartz outside the UV-photodeposited stripe. Where the CO_2 laser beam spot intersected the stripe, however, the stripe has been thickened to ~100 nm.

IV. CONCLUSIONS

Photolithographic techniques, based on image projection with visible/near-UV radiation, have attained a major role in integrated circuit manufacturing because they provide a unique combination of high precision, high volume, and low cost. The perfection of these techniques and their scaling to shorter wavelengths have been key to an improving manufacturing technology for smaller devices and greater VLSI complexity. The eventual incorporation of excimer lasers, the most important deep-UV sources to be developed in recent times, is viewed by the authors and many others as the inevitable progression of this technology. We believe, moreover, that this incorporation of excimers into circuit manufacturing will take a surprisingly broad range of directions, in the course of which projection optical technology will be applied beyond what is traditionally construed as lithography.

In this paper we have reviewed the current status and remaining technical issues for the optical and material systems which will make up this future technology. In the laboratory environment 0.13-μm lines and spaces, a factor of ~5 smaller than those obtained with current production steppers, have been demonstrated. A number of factors will de-

termine the extent to which this dimension will be approached in practical manufacturing over the next years.

There are four key, not-yet-resolved issues for excimer stepper optics. The first is the trade-off of shorter wavelength and larger numerical aperture scaling, as mediated by depth of field and material optical transmission limitations. Both λ and NA will probably be scaled to their respective practical limits. However, since the performance implications of the two quantities interact, the relative rate at which the two are scaled is not yet clear. The second key issue is the strategy for control of defocus due to chromatic aberration across the bandwidth of current lasers. Solutions to this problem variously emphasize laser or objective-lens engineering. A third issue is the control of coherence in a regime not previously encountered with lamps. A fourth, outside the main scope of this review, is the development of supporting alignment and overlay technologies for this (and all other) printing lithographies.

The materials side of the technology is much more blessed with new potential than hindered by anticipated problems. The new power of high-energy (4–7-eV) photons in resist and materials processing remains drastically underrated. This is a benefit quite outside the more widely recognized virtue of shorter wavelength scaling to achieve smaller diffraction-limited linewidth. Excimer resists will be more highly optimized for contrast, dry-etch resistance, and high-temperature processibility than current visible/near-UV materials. New material systems, including those that respond by ablation/solid-transformation and interfacial chemical reactions, will become practical and will supply new leverage in simplified and contamination-free processing.

Although the forms of the ultimate excimer projection technologies remain at best shadowy in their definition, their practical importance to mainstream electronics has now become definite. It is ironic that these techniques, after only five years of relatively relaxed development, are expected to defer alternative advanced lithographies with much longer histories (e.g., e-beam and x-ray), perhaps for a full decade.

ACKNOWLEDGMENTS

The authors would like to thank J. G. Black, J. H. Bruning, B. J. Lin, D. A. Markle, and F. Y. Wu for discussions and critical comments. This work was sponsored by the Department of the Air Force, in part under a specific program supported by the Air Force Office of Scientific Research, by the Defense Advanced Research Projects Agency and by the Army Research Office.

[1]G. M. Dubroeucq and D. Zahorsky, in Proceedings of the International Conference on Engineering, Paris, 1982, p. 73.
[2]A measure of the growing recognition is the rapidly increasing volume of publications on the subject. See, for instance, Proc. SPIE 774 (1987) and Nikkei Microdevices **1987** (2) (in Japanese).
[3]M. Rothschild and D. J. Ehrlich, J. Vac. Sci. Technol. B **5**, 389 (1987).
[4]J. A. Underhill, D. L. Sundling, and M. L. Kerbaugh, J. Vac. Sci. Technol. B **5**, 299 (1987); D. A. Markle, Proc. SPIE **774**, 108 (1987).
[5]H. L. Stover, Proc. SPIE **633**, 2 (1986).
[6]T. R. Loree, K. B. Butterfield, and D. L. Barker, Appl. Phys. Lett. **32**, 171 (1978).
[7]J. Reintjes, Opt. Lett. **5**, 342 (1980).
[8](a) V. Pol, J. H. Bennewitz, G. C. Escher, M. Feldman, V. A. Firtion, T. E. Jewell, B. E. Wilcomb, and J. T. Clemens, Proc. SPIE **633**, 6 (1986); (b) V. Pol, J. H. Bennewitz, T. E. Jewell, and D. W. Peters, Opt. Eng. **26**, 311 (1987).
[9]M. Endo, M. Sasago, Y. Hirai, K. Ogawa, and T. Ishihara, Proc. SPIE **774**, 138 (1987).
[10]M. Nakase, T. Sato, M. Nonaka, I. Higashikawa, and Y. Horiike, Proc. SPIE **773**, 226 (1987).
[11]M. Kameyama and K. Ushida, Proc. SPIE **774**, 147 (1987).
[12]R. T. Kerth, K. Jain, and M. R. Latta, IEEE Electron Device Lett. **7**, 299 (1986).
[13]D. J. Ehrlich, J. Y. Tsao, and C. O. Bozler, J. Vac. Sci. Technol. B **3**, 1 (1985).
[14]W. H. Steel, J. Opt. Soc. Am. **47**, 405 (1957).
[15]A. Offner, Photogr. Sci. Eng. **23**, 375 (1979).
[16]For a computer simulation of the two-dimensional case, see A. C. Liu and B. J. Lin, IEEE Trans. Electron Devices **30**, 1251 (1983).
[17]R. E. Kinzly, J. Opt. Soc. Am. **55**, 1002 (1965).
[18]E. C. Kintner and R. M. Sillitto, Opt. Acta **24**, 591 (1977).
[19]This result is based on the analysis of B. A. Sotskii and A. M. Goncharenko, Opt. Spectrosc. **19**, 435 (1965).
[20]D. Kohler, W. L. Seitz, T. R. Loree, and S. D. Gardner, Opt. Commun. **12**, 24 (1974).
[21]Y. Horiike, R. Yoshikawa, M. Nakase, H. Okano, H. Komano, and T. Takigawa, presented at the 1986 Fall Meeting of the Materials Research Society, Boston, 1–6 Dec. 1986, paper B&C1.2.
[22]A related method is described by D. J. Cronin and A. E. Smith, Opt. Eng. **12**, 50 (1973).
[23]M. C. King, in *VLSI Electronics: Microstructure Science*, edited by N. G. Einspruch (Academic, New York, 1981), Vol. 1, p. 41. Note that King uses a base-e logarithm, and therefore his values of γ are smaller than ours by $\log_e 10 \simeq 2.3$.
[24]B. F. Griffing and P. R. West, IEEE Electron Device Lett. **4**, 14 (1983).
[25]W. G. Oldham, IEEE Trans. Electron Devices **34**, 247 (1987).
[26]D. J. Ehrlich and J. Y. Tsao, Appl. Phys. Lett. **44**, 267 (1984).
[27]Pulse-to-pulse stability of $\pm 1\%$ has been achieved at 248 and 351 nm. U. Sengupta (private communication).
[28]S. Rice and K. Jain, IEEE Trans. Electron Devices **31**, 1 (1984).
[29]G. M. Davis and M. C. Gower, IEEE Electron Device Lett. **7**, 343 (1986).
[30]K. J. Polasko, D. J. Ehrlich, J. Y. Tsao, R. F. W. Pease, and E. E. Marinero, IEEE Electron Device Lett. **5**, 24 (1984).
[31]B. D. Grant, N. J. Clecak, R. J. Twieg, and C. G. Willson, IEEE Trans. Electron Devices **28**, 1300 (1981).
[32]K. J. Orvek, S. R. Palmer, C. M. Garza, and G. E. Fuller, Proc. SPIE **631**, 83 (1986).
[33]D. C. Hofer, K. Jain, and R. D. Miller, IBM Tech. Discl. Bull. **26**, 5683 (1984).
[34]T. M. Wolf, R. L. Hartless, A. Shugard, and G. N. Taylor, J. Vac. Sci. Technol. B **5**, 396 (1987).
[35]R. Srinivasan and V. Mayne-Banton, Appl. Phys. Lett. **41**, 576 (1982).
[36]S. Rice and K. Jain, Appl. Phys. A **33**, 195 (1984).
[37]B. Danielzik, N. Fabricius, M. Rowekamp, and D. von der Linde, Appl. Phys. Lett. **48**, 212 (1986).
[38]H. S. Cole, Y. S. Liu, H. R. Phillipp, and R. Guida, Mater. Res. Soc. Symp. Proc. **72**, 241 (1986).
[39]G. Koren, Appl. Phys. Lett. **50**, 1030 (1987).
[40]T. F. Deutsch and M. W. Geis, J. Appl. Phys. **54**, 7201 (1983).
[41]M. Latta, R. Moore, S. Rice, and K. Jain, J. Appl. Phys. **56**, 586 (1984).
[42]J. G. Black, D. J. Ehrlich, M. Rothschild, S. P. Doran, and J. H. C. Sedlacek, J. Vac. Sci. Technol. B **5**, 419 (1987).
[43]J. H. Bruning, J. Vac. Sci. Technol. **17**, 1147 (1980).
[44]J. E. Andrew, P. E. Dyer, R. D. Greenough, and P. H. Key, Appl. Phys. Lett. **43**, 1076 (1983).
[45]J. G. Black, S. P. Doran, M. Rothschild, and D. J. Ehrlich, Appl. Phys. Lett. **50**, 1016 (1987).
[46]G. Koren, F. Ho, and J. J. Ritsko, Appl. Phys. A **40**, 13 (1986).
[47]V. H. Houlding, N. J. Slattery, K. W. Beeson, and J. E. Frommer, *Beam-Induced Chemical Prccesses*, edited by R. J. Von Gutfeld, J. E. Greene,

and H. Schlossberg (Materials Research Society, Pittsburgh, 1985), p. 25.
[48]M. Rothschild, C. Arnone, and D. J. Ehrlich, J. Vac. Sci. Technol. B **4**, 310 (1986).
[49]P. D. Brewer, D. McClure, and R. M. Osgood, Jr., Appl. Phys. Lett. **49**, 803 (1986).
[50]M. Rothschild and D. J. Ehrlich (unpublished).
[51]M. R. Aylett and J. Haigh, *Beam-Induced Chemical Processes*, edited by R. T. Von Gutfeld, J. E. Greene, and H. Schlossberg (Materials Research Society, Pittsburgh, 1985), p. 63.
[52]H. Yokoyama, F. Uesugi, S. Kishida, and K. Wahio, Appl. Phys. A **37**, 25 (1985).
[53]T. H. Baum, E. E. Marinero, and C. R. Jones, Appl. Phys. Lett. **49**, 1213 (1986).
[54]J. Y. Tsao and D. J. Ehrlich, Appl. Phys. Lett. **45**, 617 (1984).
[55]G. L. Loper and M. D. Tabat, J. Appl. Phys. **58**, 3649 (1985); Mater. Res. Soc. Symp. **75**, 385 (1987).
[56]J. Y. Tsao and D. J. Ehrlich, J. Cryst. Growth **68**, 176 (1984); D. J. Ehrlich and J. Y. Tsao, J. Vac. Sci. Technol. A **3**, 904 (1985).
[57]D. J. Ehrlich and J. Y. Tsao, Appl. Phys. Lett. **46**, 198 (1985).
[58]J. Y. Tsao and D. J. Ehrlich, J. Chem. Phys. **81**, 4620 (1984).
[59]G. E. Blonder, G. S. Higashi, and C. G. Fleming, Appl. Phys. Lett. **50**, 766 (1987); G. S. Higashi, G. E. Blonder, C. G. Fleming, V. R. McCrary, and V. M. Donnelly, J. Vac. Sci. Technol. B **5**, 1441 (1987).
[60]M. Rothschild, J. H. C. Sedlacek, and D. J. Ehrlich, Appl. Phys. Lett. **49**, 1554 (1986); J. Vac. Sci. Technol. B **5**, 1400 (1987).
[61]K. Jain and R. T. Kerth, Appl. Opt. **23**, 648 (1984).
[62]P. E. Dyer and J. Sidhu, Opt. Lasers Eng. **6**, 67 (1985).
[63]B. J. Lin, J. Vac. Sci. Technol. **12**, 1317 (1975).
[64]A. M. Hawryluk, H. I. Smith, R. M. Osgood, and D. J. Ehrlich, Opt. Lett. **7**, 402 (1982).
[65]M. Tsuda, S. Oikawa, Y. Nakamura, H. Nagata, A. Yokota, H. Nakane, T. Tsumori, Y. Nakane, and T. Mifune, Photogr. Sci. Eng. **23**, 290 (1979).
[66]E. Gipstein, A. C. Ouano, and T. Tompkins, J. Electrochem. Soc. **129**, 201 (1982).
[67]H. Hiraoka, W. L. Welsh, Jr., and J. Bargon, J. Vac. Sci. Technol. B **1**, 1062 (1983).